Journal of Biomolecular NMR, 6 (1995) 113–122
ESCOM

J-Bio NMR 283

Backbone dynamics of (1–71)- and (1–36)bacterioopsin studied by two-dimensional ^{1}H-^{15}N NMR spectroscopy

Vladislav Yu. Orekhov, Konstantine V. Pervushin, Dmitry M. Korzhnev and Alexander S. Arseniev*

Shemyakin and Ovchinnikov Institute of Bioorganic Chemistry, Russian Academy of Sciences, Ul. Miklukho-Maklaya 16/10, Moscow 117871, Russia

Received 8 December 1994
Accepted 31 March 1995

Keywords: Bacteriorhodopsin; Conformational exchange; Dynamics; Helix–helix interaction; Micelles; Relaxation; Spatial structure

Summary

The backbone dynamics of uniformly ^{15}N-labelled fragments (residues 1–71 and 1–36) of bacterioopsin, solubilized in two media (methanol–chloroform (1:1), 0.1 M $^{2}HCO_2NH_4$, or SDS micelles) have been investigated using 2D proton-detected heteronuclear ^{1}H-^{15}N NMR spectroscopy at two spectrometer frequencies, 600 and 400 MHz. Contributions of the conformational exchange to the transverse relaxation rates of individual nitrogens were elucidated using a set of different rates of the CPMG spin-lock pulse train and were essentially suppressed by the high-frequency CPMG spin-lock. We found that most of the backbone amide groups of (1–71)bacterioopsin in SDS micelles are involved in the conformational exchange process over a rate range of 10^{3} to 10^{4} s^{-1}. This conformational exchange is supposed to be due to an interaction between two α-helixes of (1–71)bacterioopsin, since the hydrolysis of the peptide bond in the loop region results in the disappearance of exchange line broadening. ^{15}N relaxation rates and ^{1}H-^{15}N NOE values were interpreted using the model-free approach of Lipari and Szabo [Lipari, G. and Szabo, A. (1982) *J. Am. Chem. Soc.*, **104**, 4546–4559]. In addition to overall rotation of the molecule, the backbone N-H vectors of the peptides are involved in two types of internal motions: fast, on a time scale < 20 ps, and intermediate, on a time scale close to 1 ns. The intermediate dynamics in the α-helical stretches was mostly attributed to bending motions. A decrease in the order parameter of intermediate motions was also observed for residues next to Pro^{50}, indicating an anisotropy of the overall rotational diffusion of the molecule. Distinctly mobile regions are identified by a large decrease in the order parameter of intermediate motions and correspond to the N- and C-termini, and to a loop connecting the α-helixes of (1–71)bacterioopsin. The internal dynamics of the α-helixes on the millisecond and nanosecond time scales should be taken into account in the development of a model of the functioning bacteriorhodopsin.

Introduction

For many years, measurements of ^{15}N and ^{13}C relaxation rates have been used for NMR studies of molecular mobility (Abragam, 1961). However, only since 2D experiments with 'reverse' proton detection have been developed (Bax et al., 1989) and ^{15}N- and ^{13}C-enriched proteins have become readily available, it has been possible to perform detailed and extensive heteronuclear relaxation studies on proteins (for a recent review, see Wagner (1993)).

Internal motions faster than the rotational correlation time can be elucidated by analysis of heteronuclear relaxation rates and NOEs (Lipari and Szabo, 1982). Slow conformational exchange in the micro–millisecond time range could increase the transverse relaxation rate. The size of this increase depends on the chemical shift refocusing scheme used during the relaxation delay. Exchange processes on the millisecond time scale could be elucidated by variation of the delay between the 180° pulses in the CPMG pulse train and the exchange rates can thus be

*To whom correspondence should be addressed.

Abbreviations: BO, bacterioopsin; 2D, two-dimensional; CPMG, Carr–Purcell–Meiboom–Gill (Carr and Purcell, 1954); SDS, sodium dodecyl($^{2}H_{25}$) sulfate; $R(S_1)$, $R(S_2)$, ^{15}N transverse and longitudinal relaxation rates, respectively.

measured (Bloom et al., 1965; Reeves, 1975; Orekhov et al., 1994). The contribution to the transverse relaxation rate caused by conformational exchange on a faster (microsecond) time scale can be evaluated by measuring relaxation rates at different magnetic field strengths (Barchi et al., 1994). Thus, NMR spectroscopy can provide fundamental information on intramolecular motions in a wide range of time scales.

By now it is generally believed that membrane proteins possess a flexible spatial structure and exhibit strong conformational dynamics on very broad time scales (Popot et al., 1993), so they are very attractive objects for exploration by dynamic NMR. Comparison of the dynamic parameters of a membrane protein along with its spatial structure in different environments could give insight into protein–protein and protein–membrane interactions in lipid membranes.

Bacteriorhodopsin (or bacterioopsin (BO) for the protein without the retinal chromophore) is a transmembrane protein acting as a light-dependent proton pump in the purple membrane of *H. halobium* (see Ovchinnikov (1982) for a review). Electron cryomicroscopy data suggested a seven-α-helix structural motif for bacteriorhodopsin (Henderson et al., 1990).

High-resolution NMR studies of membrane proteins require their solubilization in a membrane-mimicking environment, i.e., an appropriate organic solvent or detergent micelles (Arseniev et al., 1987; Pervushin et al., 1991). From CD (Arseniev et al., 1987) and FT-IR (Torres and Padros, 1993) results, it was concluded that bacteriorhodopsin retains most of its native secondary structure in methanol–chloroform (1:1), 0.1 M $LiClO_4$. It was also shown that some elements of the bacteriorhodopsin native tertiary structure are present in this milieu (Arseniev et al., 1987; Abdulaeva et al., 1991). The detailed structures of bacteriorhodopsin fragments have been obtained by 2D ^1H NMR spectroscopy (Arseniev et al., 1988; Maslennikov et al., 1990,1991a,1993; Barsukov et al., 1992; Sobol et al., 1992). The spatial structures of segments A (residues 1–36) and B (residues 34–65), both in organic mixture and in sodium dodecyl($^2H_{25}$) sulfate (SDS) micelles, were reconstructed using the available NMR data (Maslennikov et al., 1991b; Lomize et al., 1992; Pervushin et al., 1992; Pervushin and Arseniev, 1992).

Here we present a ^{15}N NMR study of the backbone dynamics of the (1–71) and (1–36) fragments of bacterioopsin in methanol–chloroform (1:1), 0.1 M $^2HCO_2NH_4$, and in SDS micelles at two spectrometer frequencies, i.e., 400 and 600 MHz. The (1–36)- and (1–71)bacterioopsin fragments reveal the same structural properties as in the whole bacteriorhodopsin molecule and could be regarded as minimal structural units consisting of one 'free' α-helix and two interacting transmembrane α-helixes, respectively.

Materials and Methods

The uniformly ^{15}N-labeled fragments (1–36)- and (1–71)-bacterioopsin were isolated as described previously (Abdulaeva et al., 1987; Orekhov et al., 1992) from uniformly ^{15}N-labeled *H. halobium*, strain ET1001, which was cultured according to the published procedure (Crespi, 1982) in a medium containing the hydrolysate of ^{15}N-labeled *Chlorella vulgaris*. NMR samples were prepared as described (Pervushin et al., 1994). The Asp^{36}-Pro^{37} peptide bond of (1–71)BO in SDS micelles was hydrolysed by incubation of the NMR sample for several months at room temperature. Electrophoresis indicated almost 100% hydrolysis.

The ^{15}N and ^1H resonance assignment of (1–71)BO (Pervushin et al., 1994) was used throughout. The ^{15}N assignment for (1–36)BO was readily obtained from the ^{15}N and ^1H resonance assignments of (1–71)BO and the ^1H assignment of (1–36)BO (Pervushin et al., 1992,1994). NMR measurements were carried out at 600 and 400 MHz on UNITY-600 and UNITY-plus-400 VARIAN spectrometers at 30 °C and 50 °C for the samples in organic mixture and in micelles, respectively. The pulse sequences used to measure ^{15}N longitudinal ($R(S_z)$) and transverse ($R(S_x)$) relaxation rates were based on those described previously (Kay et al., 1989; Clore et al., 1990a; Peng and Wagner, 1992), appropriately modified to eliminate cross-correlation between dipolar and chemical shift anisotropy relaxation mechanisms (Palmer et al., 1992). In the experiments for the measurement of the $R(S_z)$ and $R(S_x)$ relaxation rates, a delay of 1.4 s was used before each transient (2.5–5 times the longitudinal relaxation time of the backbone amide protons). Delays 2τ between the centers of the 180° pulses (the pulse length was 140 μs) in the ^{15}N CPMG spin-echo sequence during the transverse relaxation period were 0.2, 0.5, 1.0 and 2.0 ms. $R(S_z)$ and $R(S_x)$ relaxation rates were obtained using relaxation delays of 0.01, 0.1, 0.2, 0.4, 0.6, 0.9, 1.2, 1.5 and 1.8 s and 0.001, 0.02, 0.04, 0.06, 0.08, 0.10, 0.12 and 0.14 s, respectively. Sample heating during the pulse sequences was estimated by measuring the separation between the OH and CH_3 resonances in the external standard (methanol) and was found not to exceed 3 °C. The ^1H-^{15}N NOEs were measured exactly as described previously (Kay et al., 1989; Clore et al., 1990a; Orekhov et al., 1994) with a delay of 4 s before each transient. All spectra were processed by a modified version of the FELIX software (Hare Research Inc., Woodinville, WA). Cross-peak volumes were measured using the program EASY (C. Bartels, ETH Zürich, Zürich). Relaxation rates and the associated errors were calculated by the appropriate utility of the VNMR (VARIAN) software. Calculation of dynamic and chemical exchange parameters was performed by software written in-house. Calculation of the 'model-free' parameter set, ζ (i.e., S_f^2, S_s^2, τ_s and Δ_{ex}, see below), was performed by nonlinear minimization of

the penalty function χ^2 (Palmer et al., 1991):

$$\chi^2(\zeta) = \sum_{i=1}^{N} (V_i^{calc}(\zeta) - V_i^{exp})^2 / (\Delta V_i^{exp})^2 \quad (1)$$

where $V^{calc}(\zeta)$ and V^{exp} are the calculated (Abragam, 1961; Clore et al., 1990b) and experimental values, respectively, and ΔV^{exp} is the uncertainty of the experimental value. Index i runs over the experimental data set (i.e., ^{15}N $R(S_x)$, $R(S_z)$ and the ^1H-^{15}N NOE measured at all available spectrometer frequencies). For the evaluation of the uncertainty in ζ, 100 Monte Carlo trials were used with V_i^{exp} taken randomly from the interval $V_i^{exp} \pm \Delta V_i^{exp}$. Minimal and maximal values of the parameter ζ obtained by this procedure were taken as corresponding lower and upper estimates for the 'model-free' parameters.

Results and Discussion

NMR measurements

Representative 2D ^1H-^{15}N correlation spectra of (1–36)-BO and (1–71)BO are shown in Fig. 1. $R(S_z)$ and $R(S_x)$ relaxation rates along with ^1H-^{15}N NOE values are summarized in Fig. 2, demonstrating that almost complete data sets were obtained for (1–36)BO and (1–71)BO in organic mixture and in SDS micelles at 600 MHz. Measurements at 400 MHz include $R(S_z)$ and $R(S_x)$ for (1–36)-BO in SDS micelles and $R(S_x)$ for (1–71)BO in the chloroform–methanol mixture. For some of the backbone amide groups no experimental data are present (Fig. 2), owing to the weak intensity and/or overlap of corresponding cross peaks in 2D ^1H-^{15}N correlation spectra (Fig. 1).

Analysis of conformational exchange

Conformational exchange processes could contribute significantly (Δ_{ex}) to the measured transverse relaxation rates, R_m, in CPMG experiments (Bloom et al., 1965):

$$R_m = \Delta_{ex} + R^*(S_x) \quad (2)$$

where $R^*(S_x)$ is the 'chemical exchange-free' part of the transverse relaxation rate, originating from internal molecular dynamics faster than the molecule rotational correlation time and from the overall rotation of the molecule.

The contribution of conformational exchange can be evaluated in several possible ways. If the exchange rate is not very high compared to the available CPMG pulse repetition rate (i.e., the exchange rate constant is less than 10^3–10^4 s^{-1}), it is straightforward to utilize the Δ_{ex} dependence on the CPMG pulse rate (Bloom et al., 1965; Reeves, 1975; Orekhov et al., 1994). Apart from the evaluation of Δ_{ex}, this approach also provides chemical shift dispersion and exchange rate constants.

The CPMG pulse rate dependence of the ^{15}N transverse relaxation rates R_m of the backbone amides of bacterioopsin fragments is plotted in Fig. 3. It is clearly seen that only (1–71)BO in SDS micelles (Fig. 3a) exhibits line broadening due to conformational exchange on the millisecond time scale. If the interaction between two α-helixes of (1–71)BO in SDS micelles is disrupted by hydrolysis of the Asp^{36}-Pro^{37} peptide bond, the exchange line broadening disappears (Fig. 3b). This allows us to 'assign' the observed conformational exchange to a process connected with helix–helix interactions. Unfortunately, the accuracy of the data is not good enough for a quantitative estimation of chemical shift dispersions and rate constants for the conformational exchange in (1–71)BO in SDS micelles. However, as already deduced from a theoretical consideration of conformational exchange presented in a previous paper (Orekhov et al., 1994), the rate constants fall in the millisecond range. For the further model-free analysis of (1–71)BO in SDS micelles we used the average of the transverse relaxation rates measured at high CPMG pulse rate (τ=0.1, 0.25 and 0.5 ms).

If the available CPMG pulse rate is less than the exchange constant, Δ_{ex} could be obtained in the 'model-free' analysis (Clore et al., 1990b) as an adjustable parameter in a nonlinear minimization (Kay et al., 1989). This method is especially useful (Barchi et al., 1994) if the data for several spectrometer frequencies are available, because only one adjustable parameter can account for the Δ_{ex} for R_m measurements at all spectrometer frequencies:

$$\Delta_{ex}^k = \Delta_{ex}^i (\nu^k / \nu^i)^2 \quad (3)$$

where the indexes i,k correspond to different spectrometers with the frequencies ν^k and ν^i.

Calculations were made for (1–71)BO in organic mixture and for (1–36)BO both in chloroform–methanol mixture and in SDS micelles, with an adjustable exchange term introduced into the penalty function χ^2 according to Eqs. 2 and 3. Table 1 lists Δ_{ex} values obtained for the residues which exhibited statistically significant exchange line broadening.

Residue Gly^{21} of (1–36)BO in organic mixture is an interesting example of a residue exhibiting conformational exchange. From NMR data (Pervushin and Arseniev, 1992; Sobol et al., 1992) and molecular dynamics simulations (Pervushin et al., 1995), it was deduced that the carbonyl group of the Met^{20}-Gly^{21} peptide bond forms a transient hydrogen bond with the $H\gamma_1O$ group of Thr^{24}. If the lifetime of this hydrogen bond falls into the microsecond time range, this could explain the observed increase of the transverse relaxation rates of the ^{15}N nucleus of Gly^{21}. It is more difficult at this time to ascribe line broadening of the other residues in Table 1 to a specific exchange process.

Evaluation of overall correlation times

The spectral density $J_R(\omega)$ of the autocorrelation function of the vector rigidly attached to an axially symmetric

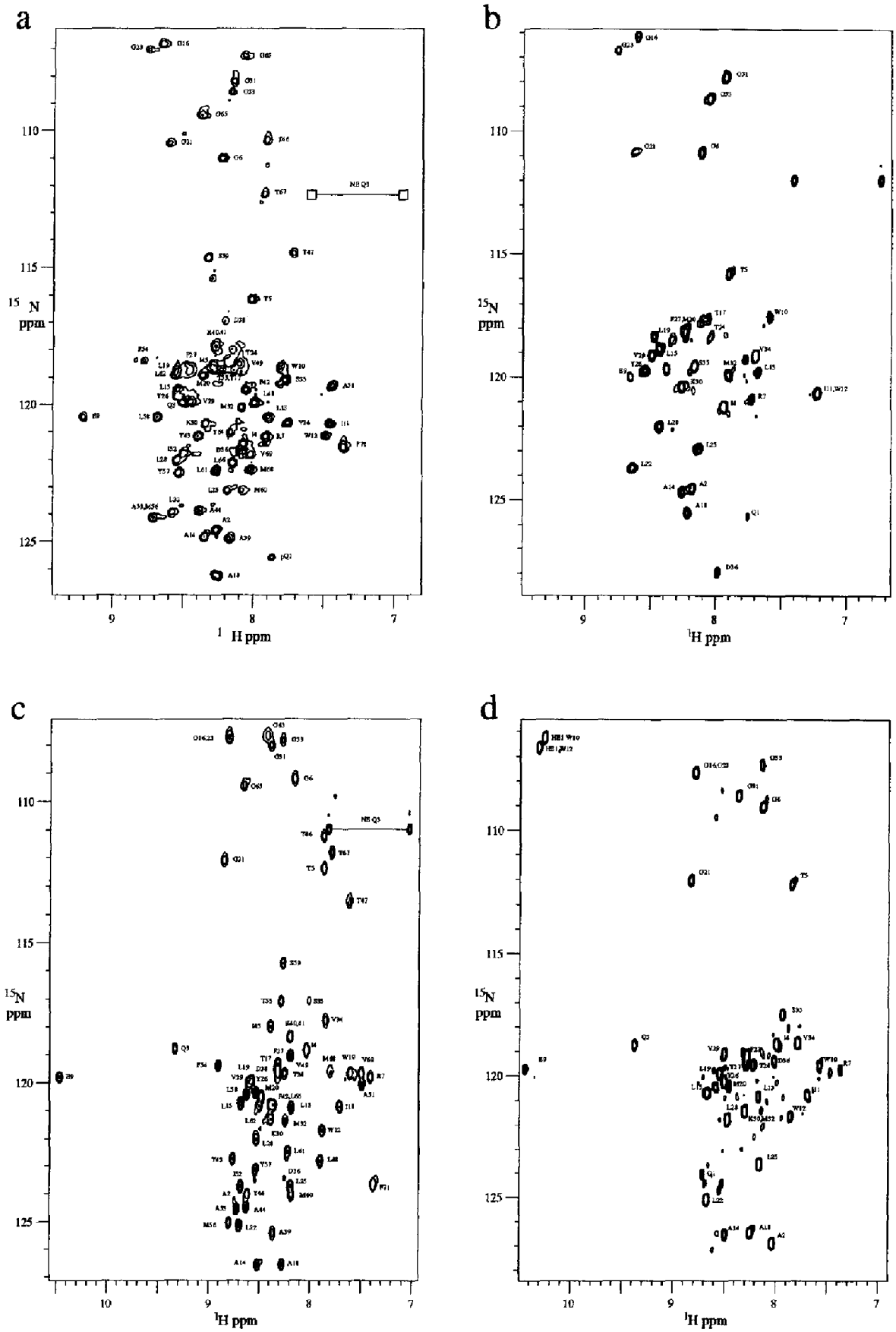

Fig. 1. ^{15}N-^{1}H HMQC spectra of uniformly ^{15}N-enriched fragments of bacterioopsin. (a) (1–71)BO in SDS micelles; (b) (1–36)BO in SDS micelles; (c) (1–71)BO in chloroform–methanol mixture; and (d) (1–36)BO in chloroform–methanol mixture.

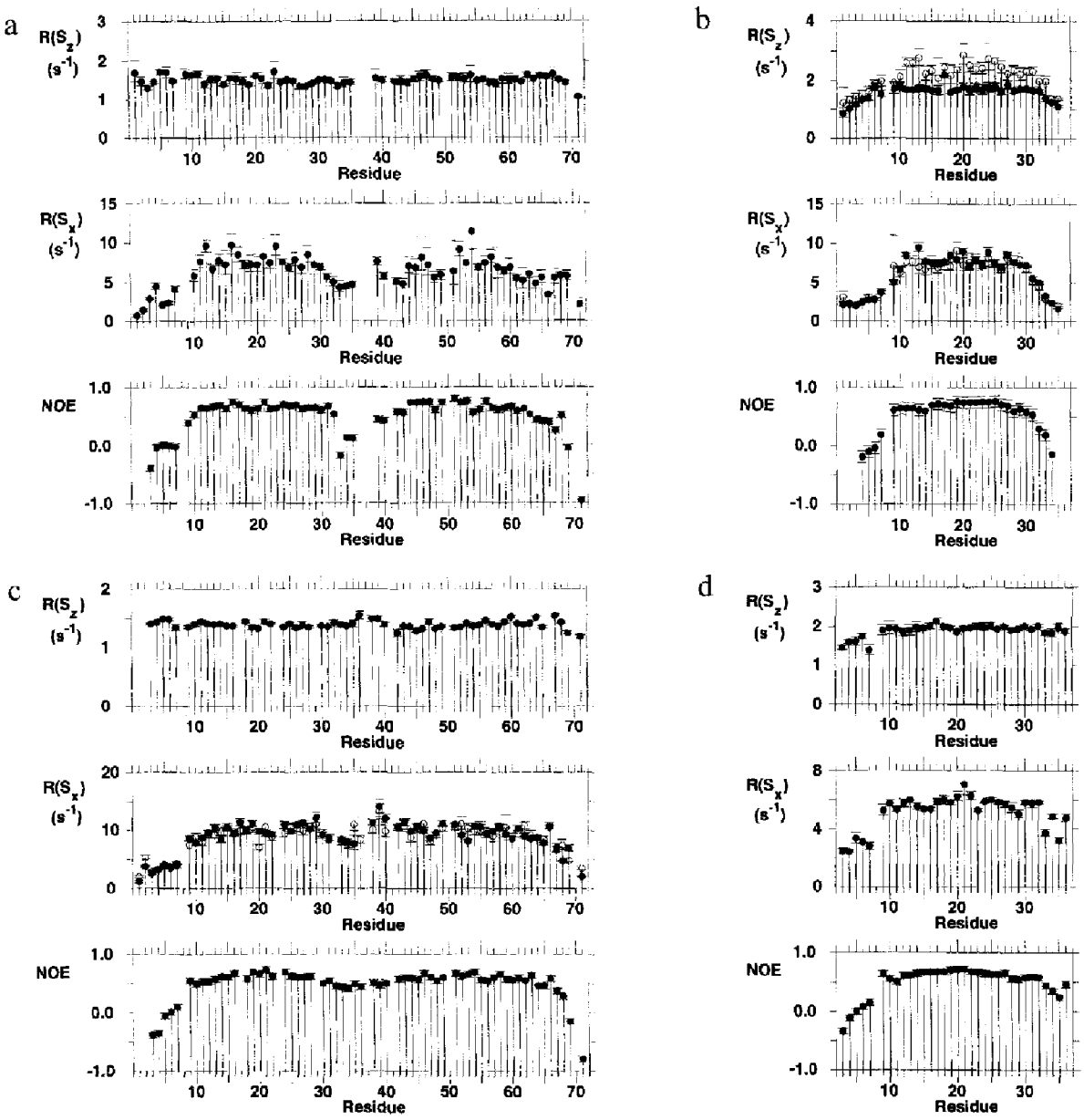

Fig. 2. Experimental ^{15}N relaxation rates and ^{1}H-^{15}N NOEs for (a) (1–71)BO and (b) (1–36)BO in SDS micelles; and (c) (1–71)BO and (d) (1–36)BO in chloroform–methanol mixture. Filled and open circles represent data for 600 and 400 MHz spectrometer frequencies, respectively.

molecule, with different rotational diffusion coefficients parallel ($D_\parallel$) and perpendicular ($D_\perp$) to the symmetry axis, is given by (Woessner, 1962,1969):

$$J_R(\omega) = \frac{2}{5}\left[\frac{A_1\tau_1}{1+\omega^2\tau_1^2} + \frac{A_2\tau_2}{1+\omega^2\tau_2^2} + \frac{A_3\tau_3}{1+\omega^2\tau_3^2}\right] \qquad (4)$$

where $A_1 = 0.75\sin^4\theta$, $A_2 = 3\sin^2\theta\cos^2\theta$, $A_3 = (1.5\cos^2\theta - 0.5)^2$, $\tau_1 = (4D_\parallel + 2D_\perp)^{-1}$, $\tau_2 = (D_\parallel + 5D_\perp)^{-1}$, $\tau_3 = (6D_\perp)^{-1}$, and θ is the angle between the vector and the diffusion ellipsoid symmetry axis. From the above equations it follows that if the vector of interest is collinear with the symmetry axis of the molecule ($\theta = 0$), the first two terms in Eq. 4 can be neglected, even in the case of strongly anisotropic motion of the molecule. Since backbone amide HN vectors are almost parallel to the axis of the α-helix of (1–36)BO, we used the isotropic $J_R(\omega)$ function for our calculation:

$$J_R(\omega) = \frac{2}{5}\frac{\tau_R}{1+\omega^2\tau_R^2} \qquad (5)$$

where τ_R is the effective overall rotational correlation time of the molecule. For the same reason, combined with the fact that the closely packed antiparallel two-α-helical motif of (1–71)BO has a more globular shape, we can use just one correlation time for the description of its overall rotational motion. The simplification of Eq. 4 to Eq. 5 is not valid for the residues situated in the terminal and loop regions (i.e., residues 1–7 and 33–36 in (1–36)BO and residues 1–7, 33–39 and 63–71 in (1–71)BO). The NH

vectors in these residues are likely to have θ values differing significantly from zero which, in principle, necessitates the use of the full form of the anisotropic spectral density function of Eq. 4. However, we used the J(ω) function of Eq. 5 to reduce the number of adjustable parameters in the model. Thus, the results obtained for these residues can be regarded only qualitatively.

The complete form of the 'isotropic' J(ω) function, including internal molecular motions, has been given by Clore et al. (1990b):

$$J(\omega)=\frac{2}{5}\left[\frac{S_f^2 S_s^2 \tau_R}{1+(\omega\tau_R)^2}+\frac{S_f^2(1-S_s^2)\tau_s'}{1+(\omega\tau_s')^2}\right] \quad (6)$$

where $1/\tau_s' = 1/\tau_R + 1/\tau_s$, τ_s is the effective correlation time for internal motions on the intermediate time scale between τ_R and the fast limit (20 ps), and S_f^2 and S_s^2 are the order parameters for motions on the fast and intermediate time scales.

If for internal motions $\tau_s < 100$ ps, then Eq. 4 can be rewritten with the order parameter S^2:

$$J(\omega)=\frac{2}{5}\left[\frac{S^2\tau_R}{1+(\omega\tau_R)^2}+\frac{(1-S^2)\tau_e'}{1+(\omega\tau_e')^2}\right] \quad (7)$$

where $1/\tau_e' = 1/\tau_R + 1/\tau_e$, τ_e is the effective correlation time for all internal motions and S^2 is the order parameter. In some cases ($\tau_e \ll \tau_R$), the relaxation data are in agreement with the simpler form of the spectral density function:

$$J(\omega)=\frac{2}{5}\frac{S^2\tau_R}{1+(\omega\tau_R)^2} \quad (8)$$

If the dynamics of most of the backbone amide vectors can be described by Eqs. 7 or 8, the value of τ_R can be obtained from the averaged ratio of $R(S_z)/R(S_x)$ (Kay et al., 1989). However, if most of the residues are involved in motions on the intermediate (nanosecond) time scale, the ratio $R(S_z)/R(S_x)$ gives an underestimated value of τ_R. Used for further calculations, the underestimated τ_R value leads to an underestimation of the value of τ_e and incorrectly suggests the selfconsistency of the calculation. For example, we consider an arbitrary macromolecule with intermediate time scale motions of NH groups ($S_f^2=0.9$, $S_s^2=0.8$, $\tau_R=7.0$ ns, $\tau_s=0.8$ ns) and calculate the relaxation rates $R(S_x)$ and $R(S_z)$ and the ^1H-^{15}N NOE values using J(ω), given by Eq. 6. The value of τ_R calculated from the ratio $R(S_z)/R(S_x)$ is 6.25 ns. Then, we investigate the behavior of the penalty function $\chi^2(S^2,\tau_e)$, obtained using the calculated relaxation rates $R(S_z)$ and $R(S_x)$ and the ^1H-^{15}N NOE values as V_i^{exp} in Eq. 2 for the different values of τ_R (see Fig. 4). It can be seen that for $\tau_R=6.25$ ns (Fig. 4a), obtained from the ratio $R(S_z)/R(S_x)$, the global minimum of χ^2 corresponds to fast internal motion ($S^2=0.812$ and $\tau_e=97$ ps). As τ_R increases, a new minimum of χ^2 appears and becomes global at $\tau_R \geq 7$ ns. This minimum corresponds to $\tau_e=1$ ns, which in turn necessitates the introduction of intermediate time scale motions, presented by the spectral density function given in Eq. 6. However, the depths of the first (at $\tau_R=6.25$ ns) and second (at $\tau_R \geq 7$ ns) minima are comparable (Fig. 4). Thus, we are not able to choose between two minima of the penalty function χ^2 and, in general, between the extreme narrowing limit of internal motions and the presence of internal dynamics on the nanosecond time scale.

To avoid this problem, additional experimental data are necessary, such as, for instance, relaxation measurements at different spectrometer frequencies. Calculations showed that τ_R values obtained from the ratio $R(S_z)/R(S_x)$ would not depend on the spectrometer frequency in the case of internal motions in the extreme narrowing limit

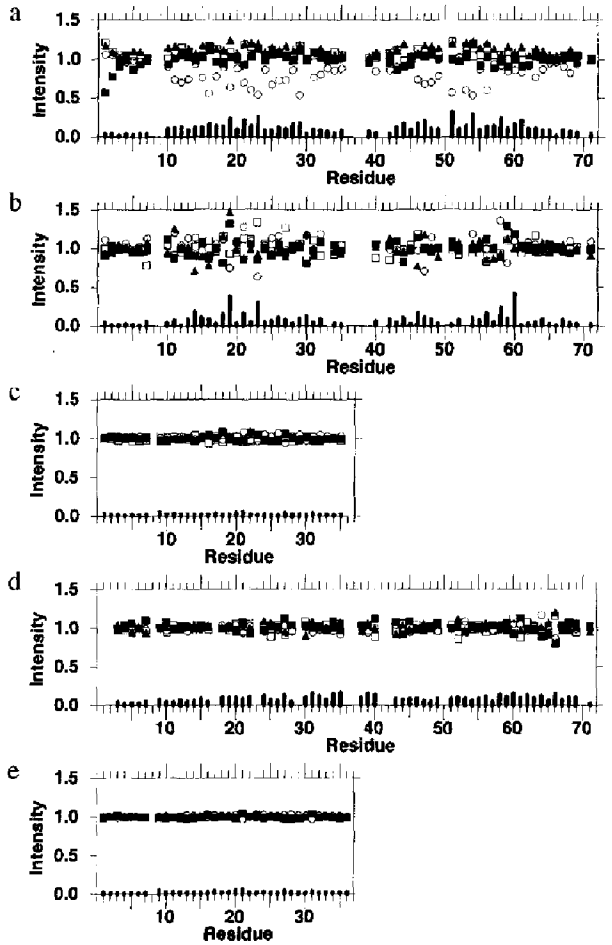

Fig. 3. The effects of conformational exchange on the transverse relaxation rate of backbone nitrogens for (1–71)BO and (1–36)BO in SDS micelles (a and c, respectively), and in chloroform–methanol mixture (d and e, respectively). Suppression of the conformational exchange for (1–71)BO after hydrolysis of peptide bond Asp^{36}-Pro^{37} is demonstrated in (b). Results are presented as normalized cross-peak intensities in $R(S_x)$ experiments (Orekhov et al., 1994) with a fixed relaxation delay T = 70 ms and different CPMG spin-echo intervals, $2\tau = 2.0$, 1.0, 0.5 and 0.2 ms (open circles, filled squares, open squares and filled triangles, respectively). Mean experimental uncertainties are shown as vertical bars at the bottom of the plots.

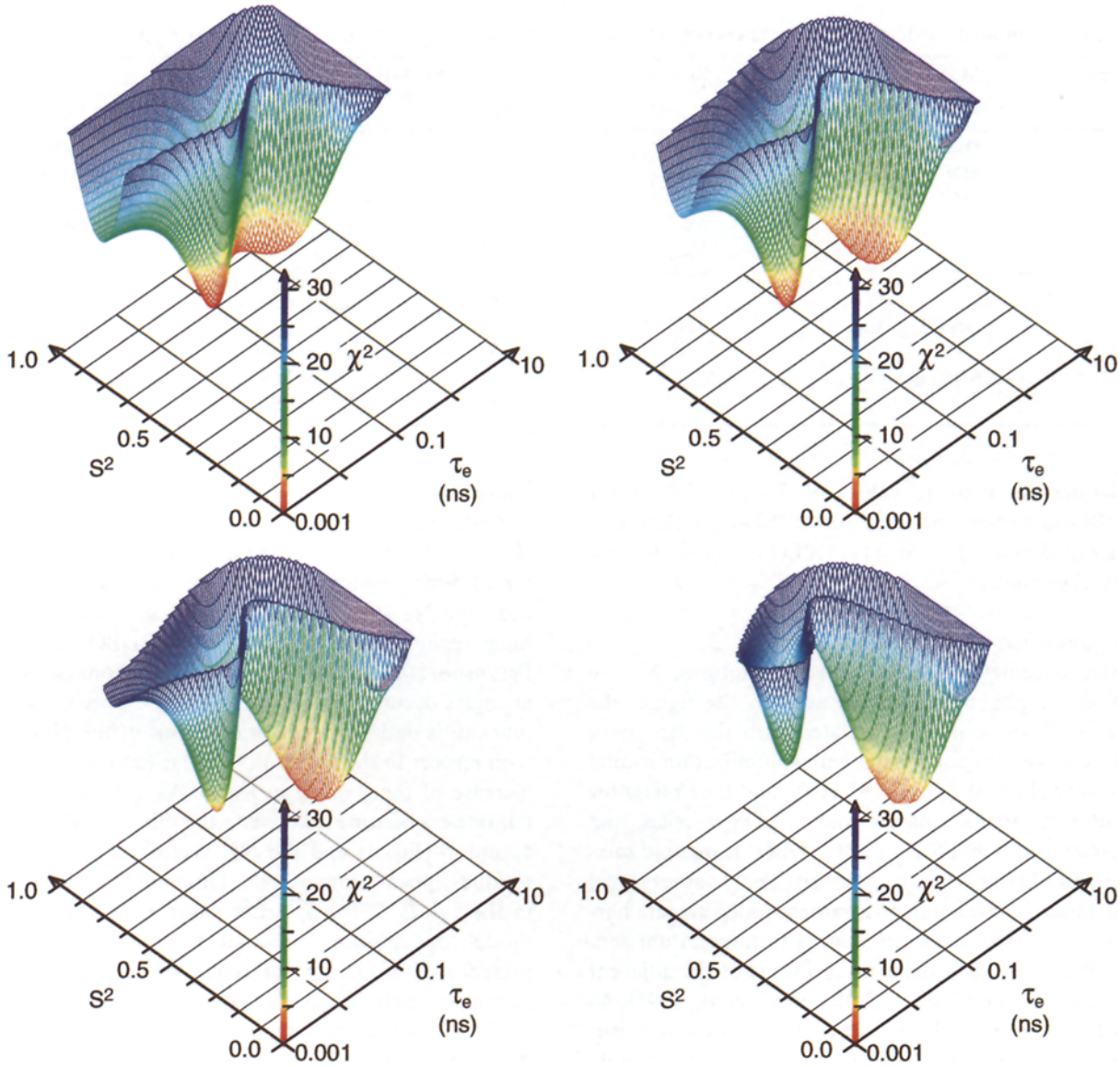

Fig. 4. Penalty function $\chi^2(S^2,\tau_e)$ (see text) versus S^2 and τ_e of Eq. 7, calculated using simulated ^1H-^{15}N relaxation rates and ^1H-^{15}N NOEs ($J(\omega)$ is given by Eq. 6, $S_f^2=0.9$, $S_s^2=0.8$, $\tau_R=7.0$ ns and $\tau_s=0.8$ ns), for values of $\tau_R=6.25$, 7.0, 7.5 and 8.0 ns (plots a, b, c and d, respectively).

($\tau_e<100$ ps), but would be lower for higher spectrometer frequencies in the case of intermediate internal motions (100 ps $<\tau_s<\tau_R$). This effect is detected for (1–36)BO in SDS micelles, where τ_R values obtained from the ratio $R(S_z)/R(S_x)$ at two spectrometer frequencies are statistically different, i.e., $\tau_R=5.6\pm0.5$ and 6.5 ± 0.6 ns for 600 and 400 MHz, respectively. A consideration of the molecular dynamics of α-helixes presented by Pervushin et al. (1994) also supports the existence of overdamped bend vibrations of the α-helixes, as well as other motions with correlation times on the intermediate time scale.

From the above reasons, we choose the spectral density function $J(\omega)$ represented by Eq. 6 for the ^{15}N NMR relaxation data analysis of α-helical fragments of bacterioopsin. τ_R values were determined by minimization of the penalty function $\Gamma(\tau_R)$, as in Orekhov et al. (1994):

$$\Gamma(\tau_R)=\sum\chi_j^2 \qquad (9)$$

where index j runs over the backbone ^{15}N nuclei under consideration and χ_j^2 is calculated assuming fast and intermediate time scale motions (Eq. 6) with the same τ_R value. It should be noted that for τ_R values larger than some 'threshold' (usually 5–10% larger than τ_R obtained from the $R(S_z)/R(S_x)$ ratio), $\Gamma(\tau_R)$ becomes virtually independent of τ_R (Fig. 5). A further increase in τ_R is compensated by the decrease of the order parameter S_s^2. Thus, the lower limit of S_s^2 and the upper limit of τ_R could be regarded only qualitatively. However, the product of $\tau_R S_s^2$ is more reliable. Since τ_R is the same for all residues (at least, if anisotropy of rotational diffusion is not taken into account), S_s^2 values could be used for the determination of the relative mobility of protein regions. For the

TABLE I
RESIDUES DISPLAYING SIGNIFICANT CONFORMATIONAL EXCHANGE Δ_{ex} IN 'MODEL-FREE' CALCULATIONS

Fragment	Medium	Residue	Δ_{ex} (s^{-1}; 600 MHz)		
			Mean	Lower	Upper
1–36	Organic mixture	Gly^{21}	0.42	0.03	1.45
1–36	SDS micelles	Leu^{13}	2.09	0.56	4.28
		Ala^{14}	1.49	0.21	3.52
		Ala^{18}	2.23	1.03	4.11
		Met^{20}	2.03	0.35	3.60
		Phe^{27}	1.34	0.28	3.02
		Met^{32}	0.85	0.29	1.66
1–71	Organic mixture	Ala^{39}	3.81	2.55	5.60
		Lys^{40}	2.72	0.26	5.70
1–71	SDS micelles	Gly^{23}	1.16	0.09	4.20
		Phe^{54}	1.49	0.30	5.90

calculations we used τ_R values of 5.0 and 7.0 ns for (1–36)BO in organic mixture and in SDS micelles, and values of 9.5 and 7.5 ns for (1–71)BO in organic mixture and in SDS micelles, respectively.

Order parameters of fast internal motions

Order parameters of fast internal motions, S_f^2, are presented in Fig. 6. As can be seen in the figure, the values of S_f^2 are scarcely correlated with the secondary structure of BO fragments and with solubilization media. The mean values of S_f^2 are 0.87 ± 0.07 and 0.82 ± 0.06 for (1–36)BO in organic mixture and in SDS micelles, and 0.87 ± 0.05 and 0.79 ± 0.07 for (1–71)BO in organic mixture and in SDS micelles, respectively. These values reveal the intrinsically local and environment-independent character of the fast motions originating from quantum zero point vibrations and stochastic collisions of the adjacent atoms (Palmer and Case, 1992; Pervushin et al., 1995). As the order parameters S_f^2 are not sensitive to the overestimation of the overall correlation time, their absolute values are in good agreement with the results provided by molecular dynamics simulations (Pervushin et al., 1995).

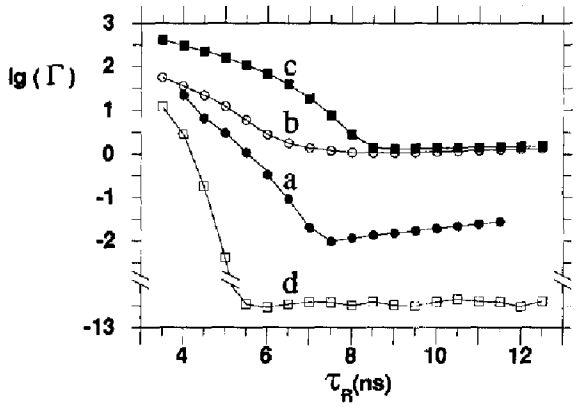

Fig. 5. $\Gamma(\tau_R)$ dependences, normalized for the number of residues taken into consideration, for (a) (1–71)BO and (b) (1–36)BO in SDS micelles; and (c) (1–71)BO and (d) (1–36)BO in chloroform–methanol mixture.

Order parameters of intermediate internal motions

Order parameters of intermediate internal motions, S_s^2 (Fig. 7), occurring on a time scale between τ_R and the fast limit (20 ps), exhibited a significant decrease for residues near the N- and C-termini for all samples, and at the hinge region and next to Pro^{50} for (1–71)BO. As noted by Pervushin et al. (1994), significant distortions of the ϕ and ψ angles occur in the vicinity of Pro^{50}. This leads to significant deviations in the orientations of the NH vectors with respect to the direction of the α-helix axis, i.e., to an increase of the θ angle in Eq. 4. As a result, relaxation parameters become sensitive to the short correlation times τ_1 and τ_2 (Eq. 4) and the NH vectors of corresponding residues appear more mobile. This could explain the drop in the values of the S_s^2 order parameters near Pro^{50}, although the additional internal dynamics induced by the presence of proline in the center of the second α-helix cannot be excluded. An analogous consideration can be made for the hinge region in (1–71)BO. However, the decrease of the order parameter in the hinge region is much more distinct in micelles than in organic solvent. If this is not an artefact caused by the misinterpretation of ^1H-^{15}N NOE data due to fast amide proton exchange with the solvent, it suggests that the loop connecting the two α-helical stretches is more flexible in SDS micelles. It can be seen in Fig. 7 that the S_s^2 order parameters decrease at the ends of all α-helixes, which is in good agreement with the theoretical consideration of α-helixes presented by Pervushin et al. (1995), where this effect was attributed to overdamped elastic rod vibrations. According to the elastic rod model (Pervushin et al., 1995), S_s^2 values should have a cosine shape, with a maximum for the residues situated in the middle of α-helixes.

Comparison of internal dynamics in one- and two-helical fragments

From the experimental results (Figs. 6 and 7), it could be derived that only minor local differences occur in the internal dynamics of the bacteriorhodopsin fragments.

Both in (1–36)BO and in (1–71)BO, a uniform distribution of S_f^2 values and a cosine shape of the S_s^2 order parameters were observed for the α-helixes. Unfortunately, due to the strong coupling of τ_R and S_s^2 and the uncertainty in τ_R, we cannot detect a uniform shift of S_s^2 between the different samples. Thus, the presence of internal dynamics, like changes of the helix–helix tilt angle as observed in molecular dynamics simulations (Pervushin et al., 1995), could not be established. In general, it may be supposed that interactions between the two α-helixes of (1–71)BO only slightly change the intrinsic α-helical motions on the nano- and picosecond time scales. However, such interactions could lead to the appearance of new types of motion on the milli- and microsecond time scales, like those observed for (1–71)BO in SDS micelles.

The results of our previous work (Orekhov et al., 1992) are in line with the present observations. Most of the cross peaks in the heteronuclear ^1H-^{15}N correlation spectra of bacteriorhodopsin in methanol–chloroform (1:1)/0.1 M $^2HCO_2NH_4$ originated from the transmembrane segments A, B and G only. The cross peaks from four segments (C, D, E and F) forming a closely packed α-helical bundle (residues 79–189) were missing, owing to conformational exchange on the millisecond time scale connected with helix–helix interactions. The absence of 40% of the expected cross peaks in the ^1H-^{15}N heteronuclear correlation NMR spectra was also noted by Seigneuret et al. (1991,1992) for bacteriorhodopsin solubilized in *n*-dodecyl maltoside detergent micelles, where the protein retains its photocycle and proton pumping activity. Thus, the dynamics occurring in bacteriorhodopsin, both in the 'quasi-native' (chloroform–methanol mixture) and in the 'native' (dodecyl maltoside micelles) state, are very complicated and include fast thermal fluctuations of atoms and bending and flickering interactions of α-helixes. In the purple membrane, bacteriorhodopsin also exhibits intramolecular rearrangements such as changing of tilts between transmembrane α-helixes (Draheim et al., 1991).

Based on these observations, we can suppose that bacteriorhodopsin comprises a set of similar structures, with slightly different modes of packing of the α-helixes. These structures interchange on the millisecond time scale. Thus, the internal dynamics of bacteriorhodopsin could be considered as a combination of the dynamics of individual α-helixes, such as bending motions, and dynamics associated with helix–helix interactions, where helixes may tilt, slide past each other, extend or shorten.

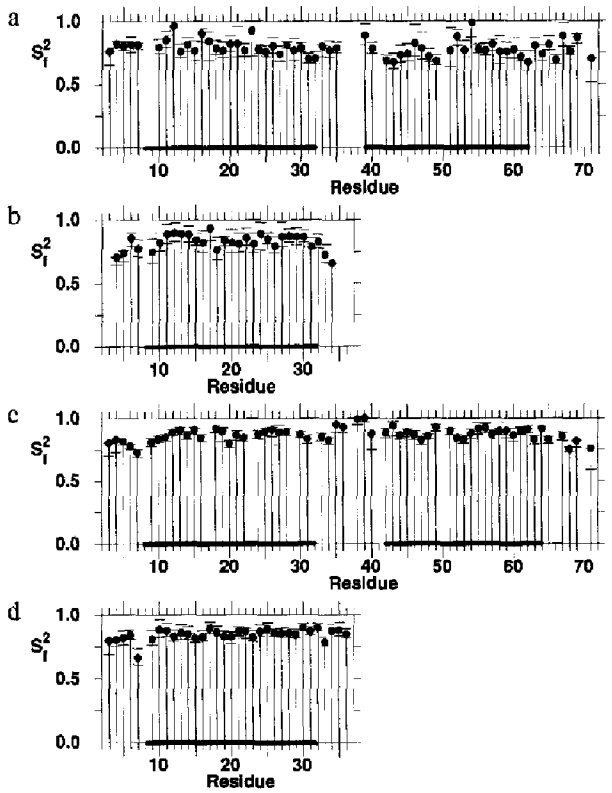

Fig. 6. Summary of S_f^2, the order parameter of fast (< 20 ps) internal motions, for (a) (1–71)BO and (b) (1–36)BO in SDS micelles; and (c) (1–71)BO and (d) (1–36)BO in chloroform–methanol mixture. The α-helical regions (Pervushin et al., 1994) are indicated by bold lines at the bottom of the plots. Short horizontal bars show upper and lower uncertainties of the order parameters.

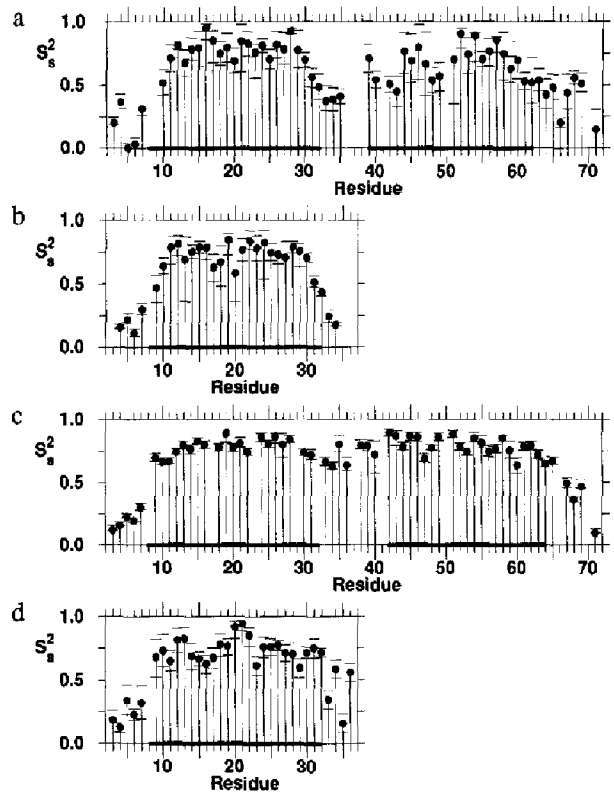

Fig. 7. Summary of S_s^2, the order parameter of nanosecond time scale internal motions, for (a) (1–71)BO and (b) (1–36)BO in SDS micelles; and (c) (1–71)BO and (d) (1–36)BO in chloroform–methanol mixture. The α-helical regions (Pervushin et al., 1994) are indicated by bold lines at the bottom of the plots. Short horizontal bars show upper and lower uncertainties of the order parameters.

Conformational dynamics of this kind could be important for proton pumping in bacteriorhodopsin, and could be a characteristic feature of other α-helical integral membrane proteins which require a conformational realignment during functioning.

Recently, Barchi et al. (1994) and Grasberger et al. (1993) tentatively attributed the effects of ^{15}N line broadening in protein spectra to the interaction between α-helix and β-strand. Thus, the conformational exchange modulated by the interaction between the elements of secondary structure could be important for proteins in general.

Conclusions

We have shown that one- and two-α-helical fragments of bacterioodopsin (residues 1–36 and 1–71) experience dynamics on a wide range of time scales. Helix–helix interactions of (1–71)BO solubilized in SDS micelles cause conformational exchange on the millisecond time scale. To account for the conformational exchange part, values of ^{15}N transverse relaxation rates along with longitudinal relaxation rates and ^{1}H-^{15}N NOE measurements were used for the characterization of internal molecular motions on the nano- and picosecond time scales. Order parameters for fast (< 20 ps) and intermediate (nanosecond) motions were calculated. The order parameters of the intermediate motions are strongly correlated with the presence of secondary structure (α-helixes) and its distortion. The dynamics observed for bacteriorhodopsin fragments could be an intrinsic feature of other membrane proteins, connected with their functioning.

Acknowledgements

This research is supported by a grant (MIP000) from the International Science Foundation.

References

Abdulaeva, G.V., Sychev, S.V. and Tsetlin, V.I. (1987) *Bioorg. Khim.*, **4**, 1254–1268.

Abdulaeva, G.V., Sobol, A.G., Arseniev, A.S., Tsetlin, V.I. and Bystrov, V.F. (1991) *Biol. Membr.*, **8**, 30–43.

Abragam, A. (1961) The Principles of Nuclear Magnetism, Clarendon Press, Oxford.

Arseniev, A.S., Kuryatov, A.B., Tsetlin, V.I., Bystrov, V.F., Ivanov, V.T. and Ovchinnikov, Yu.A. (1987) *FEBS Lett.*, **213**, 283–288.

Arseniev, A.S., Maslennikov, I.V., Kozhich, A.T., Bystrov, V.F., Ivanov, V.T. and Ovchinnikov, Yu.A. (1988) *FEBS Lett.*, **231**, 81–88.

Barchi, J.J., Grasberger, B., Gronenborn, A.M. and Clore, G.M. (1994) *Protein Sci.*, **3**, 15–21.

Barsukov, I.L., Nolde, D.E., Lomize, A.L. and Arseniev, A.S. (1992) *Eur. J. Biochem.*, **206**, 665–672.

Bax, A., Sparks, S.W. and Torchia, D.A. (1989) *Methods Enzymol.*, **176**, 134–150.

Bloom, M., Reeves, L.W. and Wells, E.J. (1965) *J. Chem. Phys.*, **42**, 1615–1624.

Clore, G.M., Driscoll, P.C., Wingfield, P.T. and Gronenborn, A.M. (1990a) *Biochemistry*, **29**, 7387–7401.

Clore, G.M., Szabo, A., Bax, A., Kay, L.E., Driscoll, P.C. and Gronenborn, A.M. (1990b) *J. Am. Chem. Soc.*, **112**, 4989–4991.

Crespi, H.L. (1982) *Methods Enzymol.*, **88**, 3–5.

Draheim, J.E., Gibson, N.J. and Cassim, J.Y. (1991) *Biophys. J.*, **60**, 89–100.

Grasberger, B.L., Gronenborn, A.M. and Clore, G.M. (1993) *J. Mol. Biol.*, **230**, 364–372.

Henderson, R., Baldwin, J.M., Ceska, T.A., Zemlin, F., Beckmann, E. and Downing, K.H. (1990) *J. Mol. Biol.*, **213**, 899–929.

Kay, L.E., Torchia, D.A. and Bax, A. (1989) *Biochemistry*, **28**, 8972–8979.

Lipari, G. and Szabo, A. (1982) *J. Am. Chem. Soc.*, **104**, 4546–4559.

Lomize, A.L., Pervushin, K.V. and Arseniev, A.S. (1992) *J. Biomol. NMR*, **2**, 361–372.

Maslennikov, I.V., Arseniev, A.S., Kozhich, A.T., Bystrov, V.F. and Ivanov, V.T. (1990) *Biol. Membr.*, **8**, 222–229.

Maslennikov, I.V., Arseniev, A.S., Chikin, L.D., Kozhich, A.T., Bystrov, V.F. and Ivanov, V.T. (1991a) *Biol. Membr.*, **8**, 156–160.

Maslennikov, I.V., Lomize, A.L. and Arseniev, A.S. (1991b) *Bioorg. Khim.*, **17**, 1456–1469.

Maslennikov, I.V., Arseniev, A.S., Chikin, L.D., Kozhich, A.T., Bystrov, V.F. and Ivanov, V.T. (1993) *Bioorg. Khim.*, **19**, 5–20.

Orekhov, V.Yu., Abdulaeva, G.V., Musina, L.Yu. and Arseniev, A.S. (1992) *Eur. J. Biochem.*, **210**, 223–229.

Orekhov, V.Yu., Pervushin, K.V. and Arseniev, A.S. (1994) *Eur. J. Biochem.*, **219**, 887–896.

Ovchinnikov, Yu.A. (1982) *FEBS Lett.*, **148**, 179–191.

Palmer, A.G., Rance, M. and Wright, P.E. (1991) *J. Am. Chem. Soc.*, **113**, 4371–4380.

Palmer, A.G. and Case, D.A. (1992) *J. Am. Chem. Soc.*, **114**, 9059–9067.

Palmer, A.G., Skelton, N.J., Chazin, W.J., Wright, P.E. and Rance, M. (1992) *Mol. Phys.*, **75**, 699–711.

Peng, J.W. and Wagner, G. (1992) *J. Magn. Reson.*, **98**, 308–332.

Pervushin, K.V., Arseniev, A.S., Kozhich, A.T. and Ivanov, V.T. (1991) *J. Biomol. NMR*, **1**, 313–322.

Pervushin, K.V. and Arseniev, A.S. (1992) *FEBS Lett.*, **308**, 190–196.

Pervushin, K.V., Sobol, A.G., Musina, L.Yu., Abdulaeva, G.V. and Arseniev, A.S. (1992) *Mol. Biol. (USSR)*, **6**, 1397–1415.

Pervushin, K.V., Orekhov, V.Yu., Popov, A., Musina, L.Yu. and Arseniev, A.S. (1994) *Eur. J. Biochem.*, **219**, 571–583.

Pervushin, K.V., Orekhov, V.Yu., Korzhnev, D.M. and Arseniev, A.S. (1995) *J. Biomol. NMR*, **5**, 383–396.

Popot, J.L. (1993) *Curr. Opin. Struct. Biol.*, **3**, 532–540.

Reeves, L.W. (1975) In *Dynamic Nuclear Magnetic Resonance Spectroscopy* (Eds, Jackman, L.M. and Cotton, F.A.), Academic Press, New York, NY, pp. 83–130.

Seigneuret, M., Neumann, J.M. and Rigaud, J.L. (1991) *J. Biol. Chem.*, **266**, 10066–10069.

Seigneuret, M., Levy, D. and Neumann, J.M. (1992) In Abstracts of the Fifth International Conference on Retinal Proteins, Dourdan, France.

Sobol, A.G., Arseniev, A.S., Abdulaeva, G.V., Musina, L.Yu and Bystrov, V.F. (1992) *J. Biomol. NMR*, **2**, 161–171.

States, D.J., Haberkorn, R.A. and Ruben, D.J. (1982) *J. Magn. Reson.*, **48**, 286–292.

Torres, J. and Padros, E. (1993) *FEBS Lett.*, **318**, 77–79.

Wagner, G. (1993) *Curr. Opin. Struct. Biol.*, **3**, 748–754.

Woessner, D. (1962) *J. Chem. Phys.*, **37**, 647–656.

Woessner, D. (1969) *J. Chem. Phys.*, **50**, 719–721.